Electronic Supplementary Information

Efficient thermally activated delayed fluorophores featuring multi-donor arms and a π-extended acceptor core

Bo Liu,[a,b] Si-Wei Chen,[a,b] Wen-Cheng Chen,*[a,b] Longjiang Xing,[a,b] Ji-Hua Tan,[a,b] Wei-Le Wu,[a,b] Xiao-Long Liu,[a,b] Jia-Xiong Chen,[a,b] Hao-Li Zhang,*[c] and Yanping Huo*[a,b,d]

[a]Guangdong Provincial Laboratory of Chemistry and Fine Chemical Engineering Jieyang Center, Jieyang, 515200, P. R. China

[b]School of Chemical Engineering and Light Industry, Guangdong University of Technology, Guangzhou, 510006, P. R. China. E-mail: wencchen@gdut.edu.cn (W.-C. Chen); yphuo@gdut.edu.cn (Y. Huo)

[c]State Key Laboratory of Applied Organic Chemistry (SKLAOC), Key Laboratory of Special Function Materials and Structure Design (MOE), College of Chemistry and Chemical Engineering, Lanzhou University, Lanzhou 730000, P. R. China. E-mail: haoli.zhang@lzu.edu.cn (H.-L. Zhang)

[d]Analytical & Testing Center, Guangdong University of Technology, Guangzhou, 510006, P. R. China

General Information

The reagents and solvents for the synthesis and measurements were used as received without further purification. NMR spectra were recorded with a Bruker Advance-400 spectrometer. Mass spectra were obtained with a Thermo Scientific Q Exactive spectrometer. Thermogravimetric analysis (TGA) was measured on a NETZSCH STA449F5 Jupiter synchronous thermal analyzer. Cyclic voltammetry (CV) was carried out on an Autolab PGSTAT302N electrochemical workstation. The electrode configuration comprises an Ag/AgCl reference electrode, a Pt wire counter electrode, and a glassy carbon working electrode. The CV scan was conducted using a tetra-*n*-butylammoniumhexafluorophosphate (Bu_4NPF_6) dichloromethane solution (0.1 M) as an electrolyte at a scan rate of 100 mV s^{-1}. Absorption spectra were recorded on a Shimadzu UV-2700 spectrophotometer. Photoluminescence (PL) spectra in solutions, low-temperature PL spectra in thin films, PL quantum yields (The Φ_p of the evaporation film was evaluated by integrating sphere in the air; The Φ_{PL} was calculated by the area integral of the PL spectra of the evaporation film before and after deoxygenation; $\Phi_d = \Phi_{PL} - \Phi_p$.), and transient PL decay were measured using an Edinburgh Instruments FLS980 spectrometer. Crystallographic data were collected at 170 K on a Rigaku Oxford Diffraction Supernova Dual Source diffractometer equipped with an Atlas S2 CCD.

Theoretical Calculations

The ground state geometries (S_0) were optimized by the density functional theory (DFT). The lowest singlet excited state (S_1) geometries were optimized by time-dependent DFT (TD-DFT). TD-DFT calculated the excited-state information at their ground state geometries and lowest singlet excited state geometries. All the above theoretical calculations were performed using the Gaussian 09 program package. The ground states were performed at B3LPY/6-31G (d) level. The excited states and natural transition orbitals (NTOs) were calculated using time-dependent TD-DFT methods (B3LYP/6-311G (d), IOP (9/40=5)) in tetrahydrofuran. The charge transfer amount of each fragment in the molecular natural transition orbital was calculated by the Multiwfn 3.7 program.[1] The frontier molecular orbital electron cloud distribution, the particle and hole distribution of the natural transition orbital, and the molecular ground state and excited state configurations were plotted by the visual molecular dynamics (VMD) program.[2]

Device fabrication and measurement

Devices were prepared on glass substrates with indium tin oxide (ITO) coating (15 Ω per square). The ITO substrates were treated with an ultrasonic bath in isopropanol and deionized water and then dried under nitrogen flow. The pre-cleaned ITO substrates experienced UV ozone treatment (20 min). Substrates were instantly loaded into a deposition chamber with a 5×10^{-7} Torr base pressure. The deposition rate of organic layers was kept at 1-2 Å s^{-1}, while those for LiF and Al deposition were 0.1 and 6 Å s^{-1}, respectively. Luminance and electroluminescence spectra were acquired from a PhotoResearch PR-745 photometer. Current density–voltage characteristics were recorded on a Keithley 2400 power source. Electroluminescence distribution was measured with an angle-dependent device testing system (C9920-11, Hamamatsu Photonics). Device measurements were performed under ambient conditions without encapsulation.

Synthesis

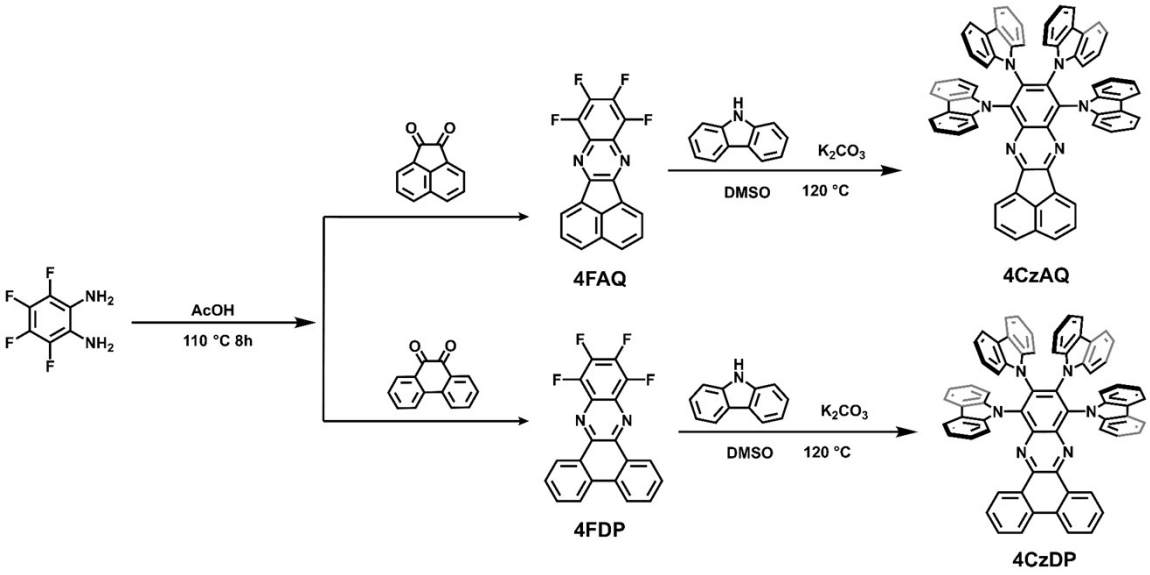

Scheme S1 Synthetic routes of **4CzAQ** and **4CzDP**.

The starting materials 3,4,5,6-tetrafluorobenzene-1,2-diamine were purchased from Bidepharm Co., Ltd (Shanghai, China) and used directly without further purification.

8,9,10,11-tetrafluoroacenaphtho[1,2-*b*]quinoxaline (4FAQ): 3,4,5,6-tetrafluorobenzene-1,2-diamine (0.18 g, 1 mmol), acenaphthylene-1,2-dione (0.18g, 1 mmol)

and 50 ml of acetic acid were added to a 150 mL two-necked flask containing a magnetic stirrer. The reaction mixture was heated to 110 °C for 8 hours under a nitrogen atmosphere. After cooling to room temperature, the mixture was poured into water, and the filter residue was collected by filtration to obtain a yellow solid 4FAQ crude product (0.27 g, 83 %), which was directly put into the next reaction without purification. ^{1}H NMR (400 MHz, $CDCl_3$) δ 8.09 (dd, *J*=5.0, 0.8, 2H), 7.97 (d, *J*=5.0, 2H), 7.71 (t, *J*=4.9, 2H).

10,11,12,13-tetrafluorodibenzo[*a*,*c*]phenazine (4FDP): The synthesis method is consistent with 4FAQ. By simply changing the substrate to phenanthrene-9,10-dione (0.2 g, 1 mmol) in the condensation stage, the orange solid 4FDP crude product (0.3 g, 85 %) was finally obtained, which could be directly used in the next step without purification.^{1}H NMR (400 MHz, $CDCl_3$) δ 8.77 (dd, *J*=4.9, 1.1, 2H), 8.19 (dd, *J*=4.9, 1.1, 2H), 7.62 (td, *J*=5.0, 1.1, 2H), 7.58 (td, *J*=5.0, 1.1, 2H).

8,9,10,11-*tetra*(9*H*-carbazol-9-yl)acenaphtho[1,2-*b*]quinoxaline (4CzAQ): 4FAQ (0.33 g, 1 mmol) and dry DMSO (20 mL) were heated in a 100 mL two-neck flask to 100 °C and stirred to dissolve. The reaction system of carbazole (0.75 g, 4.5 mmol) and K_2CO_3 (1.24 g, 9 mmol) was added and heated to 120 °C for 10 h. At the end of the reaction, the mixture was cooled to room temperature, poured into water, vacuum filtration, and the filter residue was collected to obtain a yellow solid crude product. The dark yellow solid **4CzAQ** (0.77g, 84 %) was obtained by silica gel chromatography purification column (DCM/PE, 1:2).^{1}H NMR (400 MHz, CDCl3) δ 8.07 (d, *J*=8.2, 2H), 7.93 (d, *J*=7.0, 2H), 7.84 (d, *J*=7.2, 4H), 7.68 (dd, *J*=8.2, 7.1, 2H), 7.32 (d, *J*=7.3, 4H), 7.16 – 7.01 (m, 12H), 6.98 – 6.89 (m, 4H), 6.74 (t, *J*=7.2, 4H), 6.63 – 6.53 (m, 4H). ^{13}C NMR (400 MHz, $CDCl_3$) δ 153.10, 141.68, 140.97, 138.99, 138.28, 136.37, 134.32, 126.94, 125.18, 124.50, 124.06, 123.76, 120.41, 120.33, 119.94, 119.45, 111.32, 110.49. MS (ESI): calcd for $C_{66}H_{38}N_6$ $[M]^+$ 915.07, found 915.6817.

10,11,12,13-tetra(9*H*-carbazol-9-yl)dibenzo[*a*,*c*]phenazine (4CzDP): The synthesis method is consistent with **4CzAQ**. By replacing the substrate with 4FDP (0.35 g, 1 mmol), the orange-red solid crude product was finally obtained, and the red solid **4CzDP** (0.3 g, 84 %) was purified by chromatographic column (DCM/PE, 1:2).^{1}H NMR (400 MHz, $CDCl_3$) δ 8.42 (d, *J*=8.2, 2H), 8.10 (d, *J*=8.1, 2H), 7.92 (d, *J*=7.7, 4H), 7.66 (dd, *J*=11.2, 4.1, 2H), 7.43 – 7.28 (m, 6H), 7.17 (dd, *J*=8.2, 3.7, 8H), 7.09 (t, *J*=7.4, 4H), 6.96 (t, *J*=7.7, 4H), 6.78 (t, *J*=7.4, 4H), 6.64 (t, *J*=7.7, 4H). ^{13}C NMR (400 MHz, $CDCl_3$) δ 152.95, 148.64, 142.88, 141.31, 139.79, 138.95, 137.42, 136.94, 134.46,

133.97, 127.09, 124.41, 124.21, 122.75, 122.30, 115.49, 115.05, 110.96, 110.13. MS (ESI): calcd for $C_{68}H_{40}N_6$ $[M]^+$ 941.11, found 941.5639.

Determination of Rate Constants

The prompt lifetimes were obtained by exponentially fitting the PL decay curves with mono-exponential function as $I_t = I_0 e^{-t/\tau_p}$, in which I is the photoluminescence intensity, t is decay time, and τ_p is the prompt lifetime. The experimental PL decay can be expressed with a bi-exponential function as $I_t = B_1 e^{-t/\tau_p} + B_2 e^{-t/\tau_d}$ in which B_1 and B_2 are the quantities of emission components, τ_p and τ_d are the lifetimes of prompt (p) and delayed (d) components, respectively.

The total and delayed fluorescence quantum efficiencies (Φ_{PL} and Φ_d) were determined using the prompt fluorescence quantum efficiency (Φ_p) and the relative ratios between prompt and delayed components, which were calculated from the following transient PL measurements.

When $k_{IC} << k_F$, k_{IC} can often be ignored, and nonradiative transitions of singlet excitons (k_{nr}) are considered the main loss channel due to the long lifetime before decay. The critical kinetic parameters of the **4CzAQ** and **4CzDP** doped films were calculated according to the following equations:

$$k_p = \frac{1}{\tau_p} \tag{1}$$

$$k_d = \frac{1}{\tau_d} \tag{2}$$

$$k_F = \frac{k_p k_d}{k_{RISC}} \Phi_{PL} \tag{3}$$

$$k_{ISC} = k_p(1 - \Phi_p) \tag{4}$$

$$k_{RISC} = \frac{k_p k_d \Phi_d}{k_{ISC} \Phi_p} \tag{5}$$

$$k_{nr} = \frac{k_p k_d}{k_{RISC}}(1 - \Phi_{PL}) \tag{6}$$

where τ_p and τ_d represent the prompt and delayed decay lifetimes, respectively; Φ_{PL}, Φ_p, and Φ_d are the total, prompt, and delayed fluorescence quantum efficiencies, respectively; k_p, k_{RISC}, and k_d are the rate constants of prompt fluorescence, the RISC, and delayed fluorescence decay, respectively; and k_{nr} is the nonradiative decay rate constant of singlet excitons.

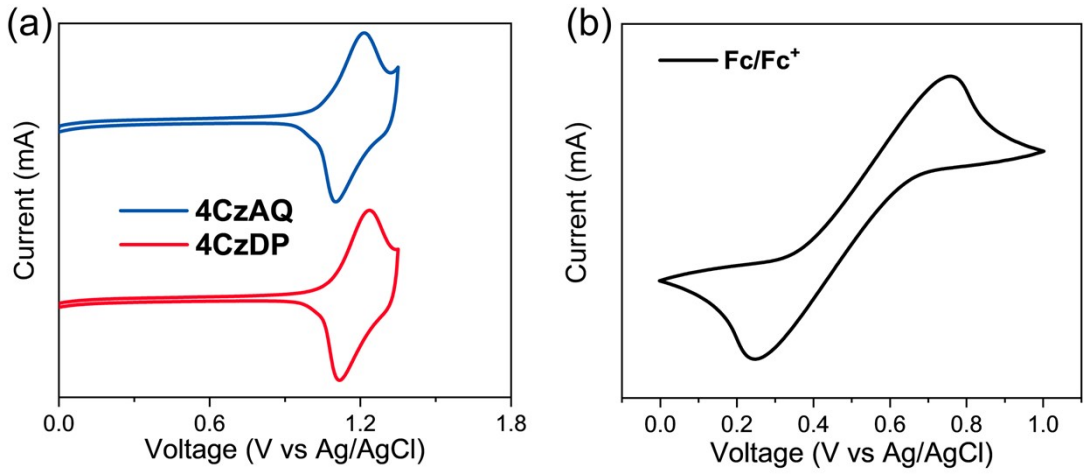

Fig. S1 Cyclic voltammogram of oxidative scans of **4CzAQ**, **4CzDP**, and ferrocene.

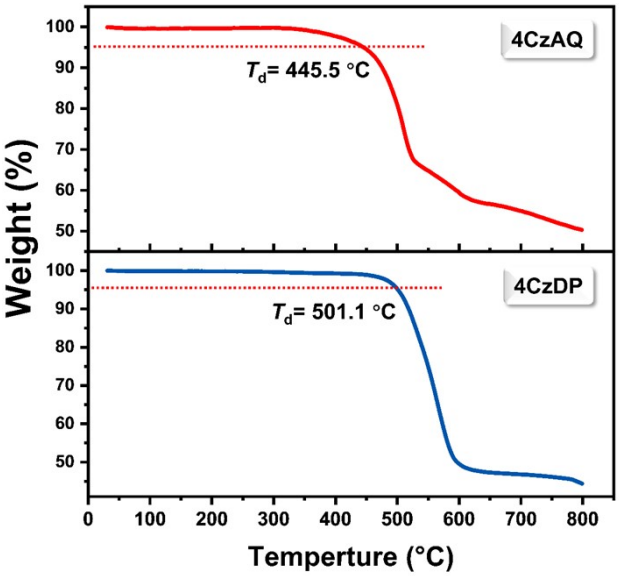

Fig. S2 The TGA curves of **4CzAQ** and **4CzDP**.

Table S1 Thermal and electrochemical data of **4CzAQ** and **4CzDP**.

Compounds	T_d (°C)	HOMO (eV)	LUMO (eV)	E_g (eV)
4CzAQ	445.5	-5.44	-2.92	2.52
4CzDP	501.1	-5.47	-3.15	2.32

Table S2 DFT optimized structures of AQ, DP, **4CzAQ** and **4CzDP**.

Compounds	HOMO (eV)	LUMO (eV)	E_g (eV)	E_{S1} (eV)	E_{T1} (eV)	ΔE_{ST} (eV)	f
AQ	-6.01	-2.03	3.98	3.50	2.37	1.13	0.055
DP	-6.03	-2.21	3.82	3.26	2.32	0.94	0.019
4CzAQ	-5.30	-2.48	1.92	2.23	2.07	0.16	0.023
4CzDP	-5.34	-2.73	2.05	2.03	1.85	0.18	0.021

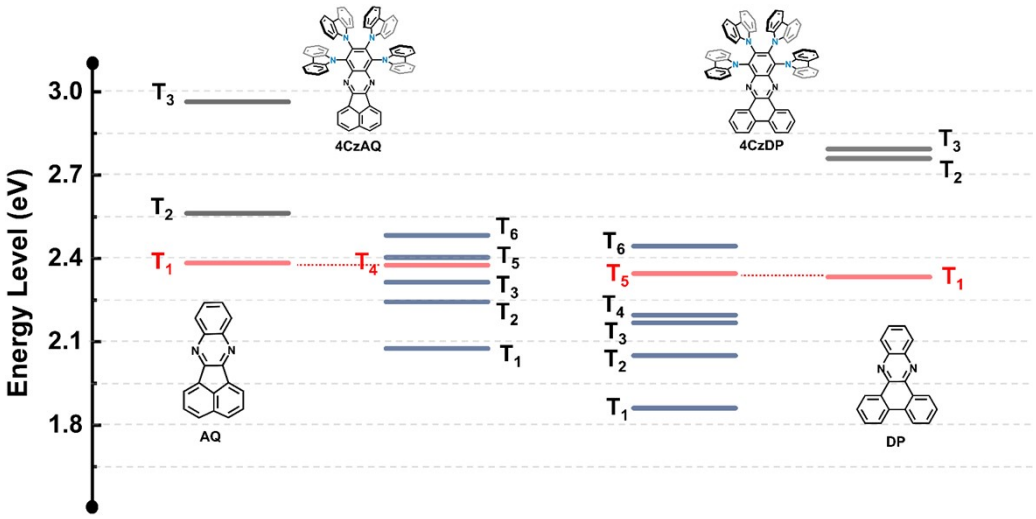

Fig. S3 Excited triplet energy levels of AQ, DP, **4CzAQ** and **4CzDP**.

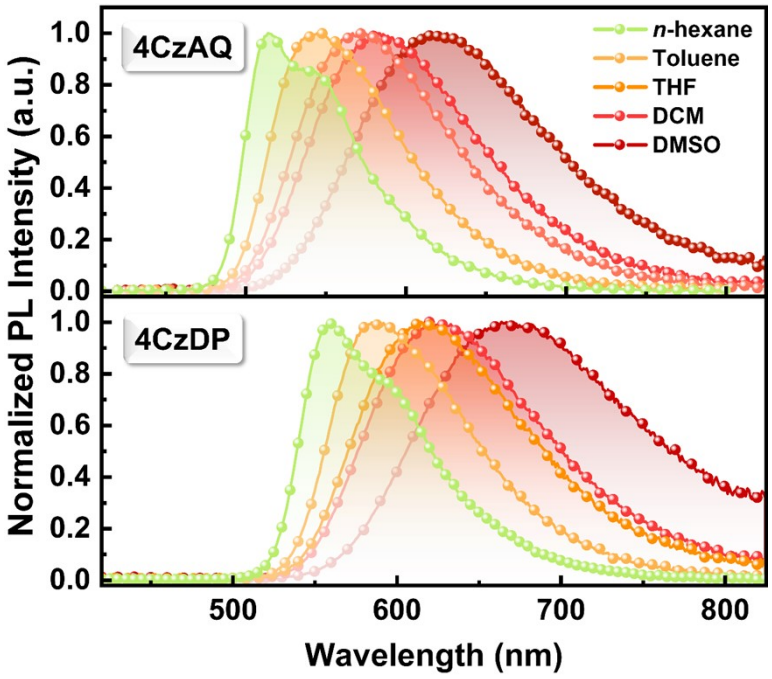

Fig. S4 PL spectra of **4CzAQ** and **4CzDP** diluted in *n*-hexane, toluene, THF, DCM and DMSO at room temperature.

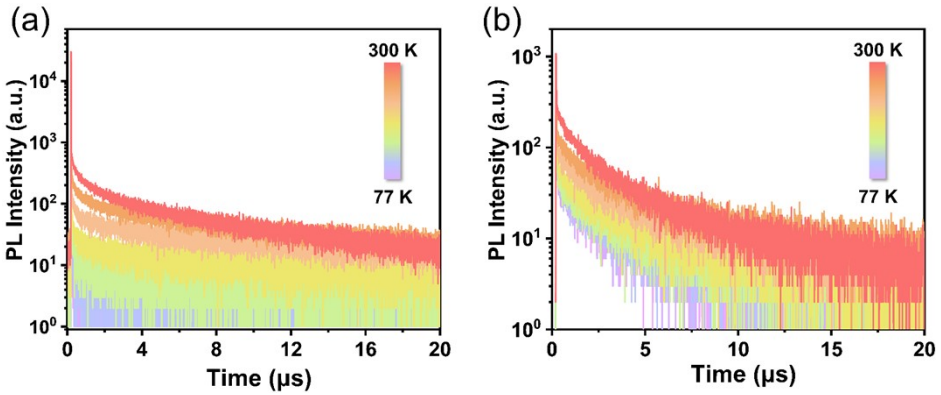

Fig. S5 Transient PL decays of (a) **4CzAQ** and (b) **4CzDP** doped film (10 wt.% in PMMA) at varying temperatures.

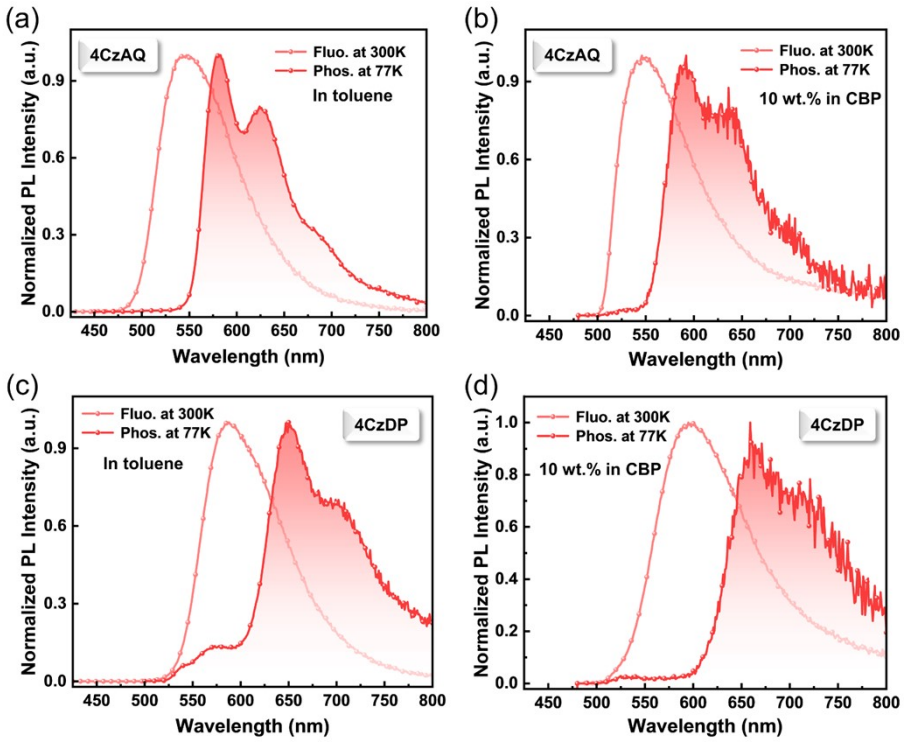

Fig. S6 (a) Fluorescence and phosphorescence spectra of **4CzAQ** diluted in toluene (10^{-5} mol L^{-1}); (b) Fluorescence and phosphorescence spectra of **4CzAQ** doped in CBP film (10 wt.%); (c) Fluorescence and phosphorescence spectra of **4CzDP** diluted in toluene (10^{-5} mol L^{-1}); (d) Fluorescence and phosphorescence spectra of 10 wt.% **4CzDP** doped in CBP film (10 wt.%).

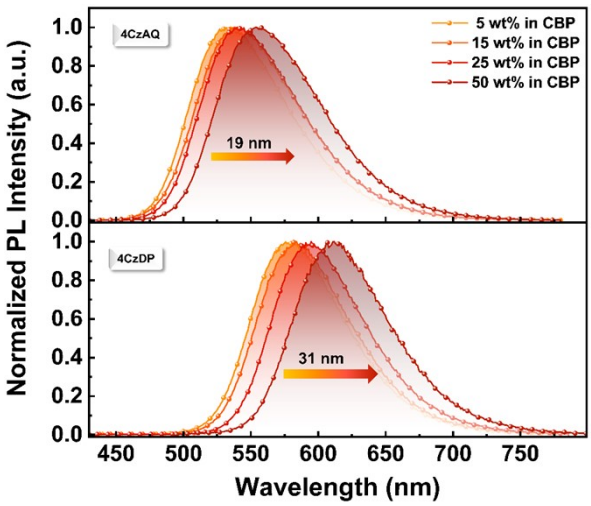

Fig. S7 The PL spectra of 5-50 wt.% doped films of **4CzAQ** and **4CzDP**.

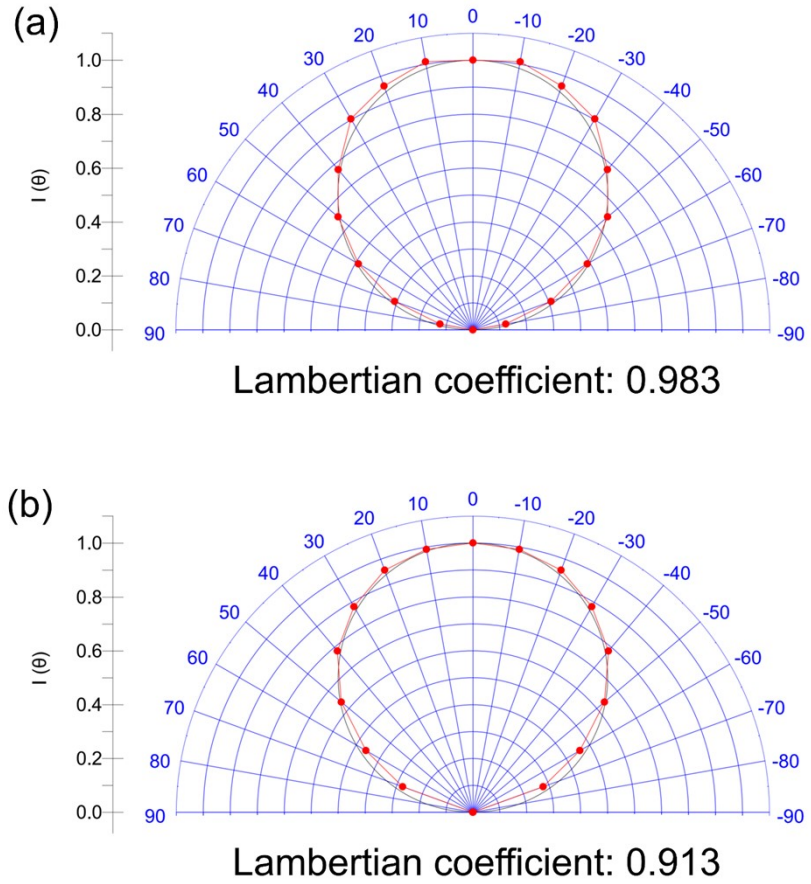

Fig. S8 Angle-dependent EL intensity profiles of 10 wt.% doped devices based on a) **4CzAQ** and b) **4CzDP**.

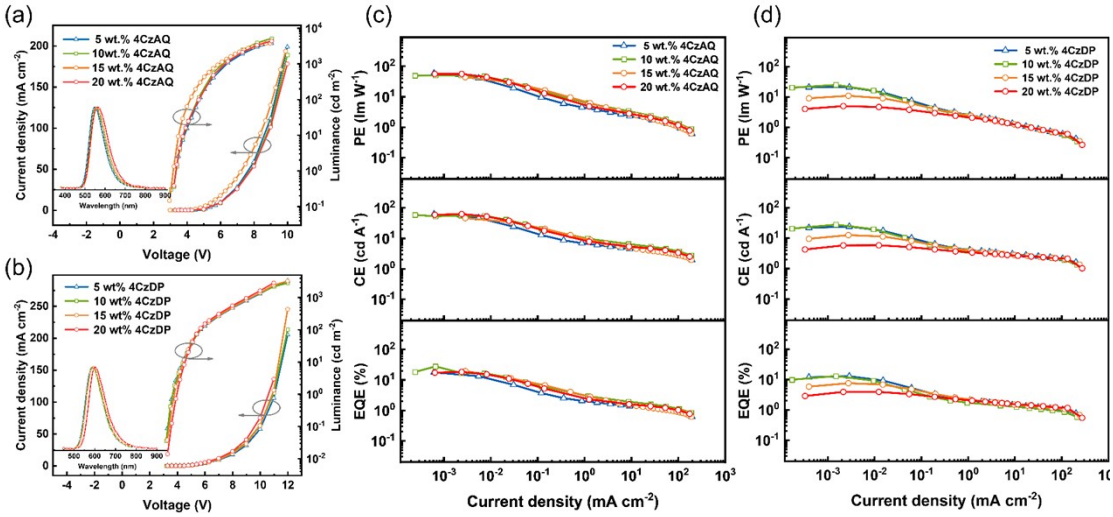

Fig. S9 (a) Current density and luminance versus driving voltage characteristics (inset: electroluminescent spectra at 100 cd m^{-2}) for **4CzAQ**. (b) Current density and luminance versus driving voltage characteristics (inset: electroluminescent spectra at 100 cd m^{-2}) for **4CzDP**. (c) Power efficiency (upper), current efficiency (middle) and external quantum efficiency (bottom) versus luminance characteristics for **4CzAQ**. (d) Power efficiency (upper), current efficiency (middle) and external quantum efficiency (bottom) versus luminance characteristics for **4CzDP**.

Table S3 Summary of OLED device performance utilizing **4CzAQ** and **4CzDP**.

Dopant	x (wt.%)	V_{on}[a] (V)	λ_{EL}[b] (nm)	CE_{max}[c] (cd A^{-1})	PE_{max}[d] (lm W^{-1})	EQE_{max}[e] (%)	CIE[f] (x, y)
4CzAQ	5	3.8	550	57.6	49.1	17.1	(0.38, 0.59)
	10	3.7	555	60.5	57.5	26.8	(0.43, 0.55)
	15	3.7	560	44.4	45	18.9	(0.44, 0.51)
	20	3.6	564	51.1	43.4	17.6	(0.41, 0.56)
4CzDP	5	3.9	594	22	19.2	11.4	(0.57, 0.42)
	10	3.8	600	25.4	22.7	11.7	(0.55, 0.44)
	15	3.7	606	11.4	10	6.8	(0.56, 0.42)
	20	3.7	616	5.3	4.6	3.5	(0.60, 0.40)

[a]Turn-on voltage at 1 cd m^{-2}. [b]EL peak wavelength at 100 cd m^{-2}. [c]Maximum current efficiency. [d]Maximum power efficiency. [e]External quantum efficiency values at maximum. [f]CIE 1931 coordinates measured at 100 cd m^{-2}.

Table S4 Electroluminescent performance of representative TADF emitters based on multi-carbazole structure.

Emitters	λ_{EL} (nm)	EQE_{max} (%)	CIE (x, y)	Reference
4CzAQ	555	26.8	(0.43, 0.55)	This work
4CzDP	600	11.7	(0.55, 0.44)	This work
4CzBN	458	10.6	(0.17, 0.20)	3
4TCzBN	463	16.2	(0.16, 0.22)	3
5CzBN	490	16.7	(0.22, 0.40)	3
5TCzBN	490	21.2	(0.21, 0.41)	3
5Cz-TRZ	486	29.3	-	4
TmCz-TRZ	496	19.7	-	4
6TBN	496	23.0	(0.09, 0.52)	5
mPyBN	496	17.3	(0.22, 0.42)	6
pCF3BN	493	15.1	(0.19, 0.40)	6
PyPhBN	501	20.6	(0.21, 0.46)	6
PyCF3BN	488	19.5	(0.18, 0.38)	6
CbPyCF3BN	494	19.6	(0.19, 0.41)	6
2CPTCB	468	21.1	(0.15, 0.19)	7
26DCPTCB	504	27.6	(0.22, 0.49)	7
5CzBP	512	12.5	(0.34, 0.58)	8
3CzDBFTrz	498	18.7	(0.19, 0.41)	9
3mCzDBFTrz	517	15.7	(0.31, 0.58)	9
26tCzPPC	497	25.4,	(0.20, 0.47)	10
246tCzPPC	491	29.6	(0.18, 0.40)	10
35tCzPPC	494	18.2	(0.19, 0.42)	10
4CzBN	458	10.91	(0.16, 0.20)	11
4CzBN-BP	474	11.80	(0.17, 0.31)	11
4CzBN-ICz	470	4.05	(0.18, 0.29)	11
5tCzMeB	481	24.6	(0.19, 0.32)	12
5tCzBP	497	12.5	(0.23, 0.41)	12
4PhCz2BN	470	22.4	(0.13, 0.15)	13

2Cz2DMAC2BN	506	20.2	-	14
5CzOXD	487	8.7	(0.18, 0.34)	15
5tCzOXD	487	14.2	(0.18, 0.37)	15
mCF35tCzOXD	494	22.1	(0.19, 0.42)	15
pCF35tCzOXD	494	20.3	(0.19, 0.41)	15
dCF35CzOXD	495	18.4	(0,20, 0.43)	15
dCF35tCzOXD	496	23.3	(0.20, 0.45)	15
4CzIPN	509	19.3	-	16
4CzTPN-Ph	578	8.0	-	16
2CzPN	471	11.2	-	16
HATNA-tCz	668	1.8	(0.66, 0.34)	17
HATNA-tPCz	692	4.8	(0.66, 0.32)	17

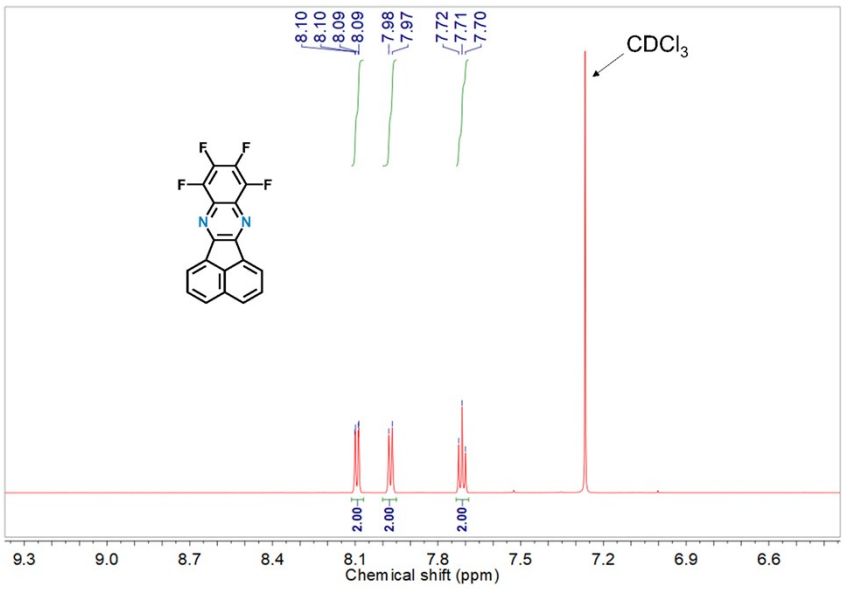

Fig. S10 ^{1}H NMR chart of 4FAQ.

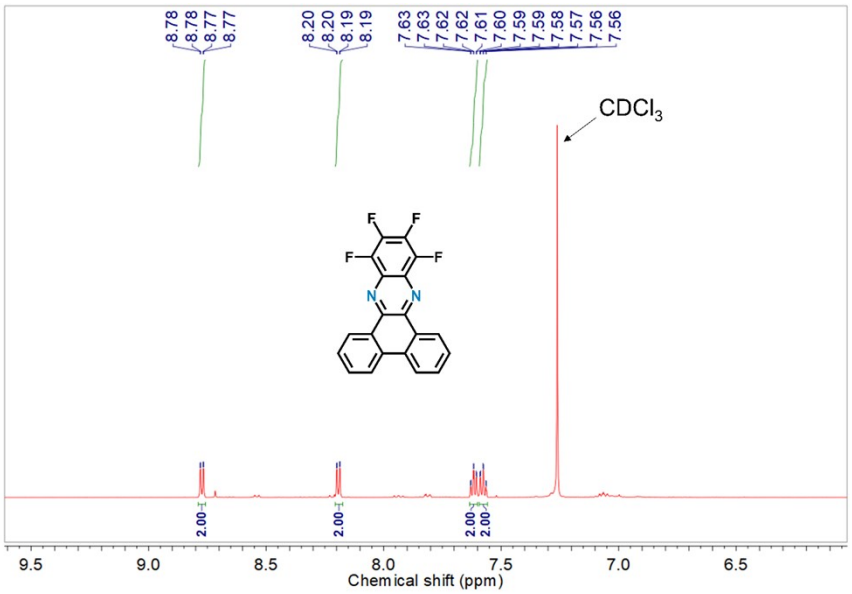

Fig. S11 ^{1}H NMR chart of 4FDP.

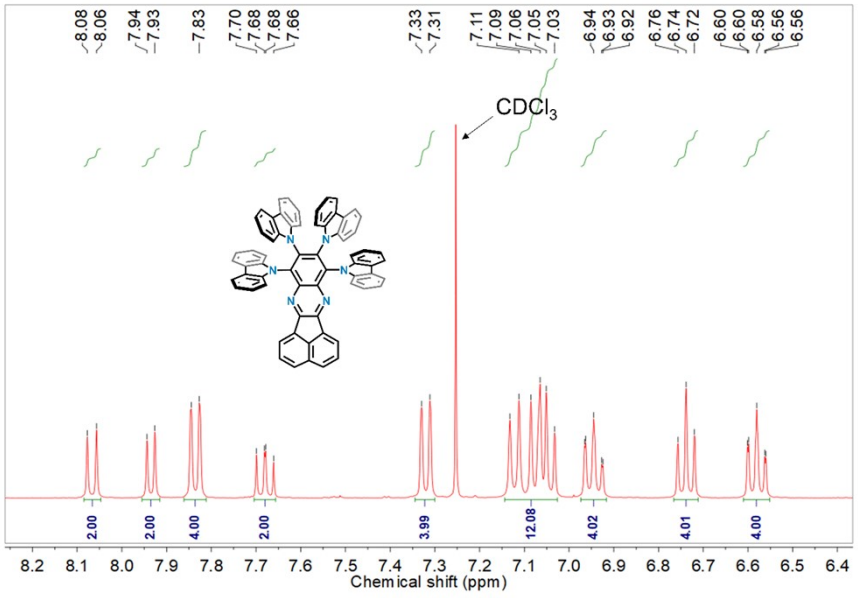

Fig. S12 ^{1}H NMR chart of **4CzAQ**.

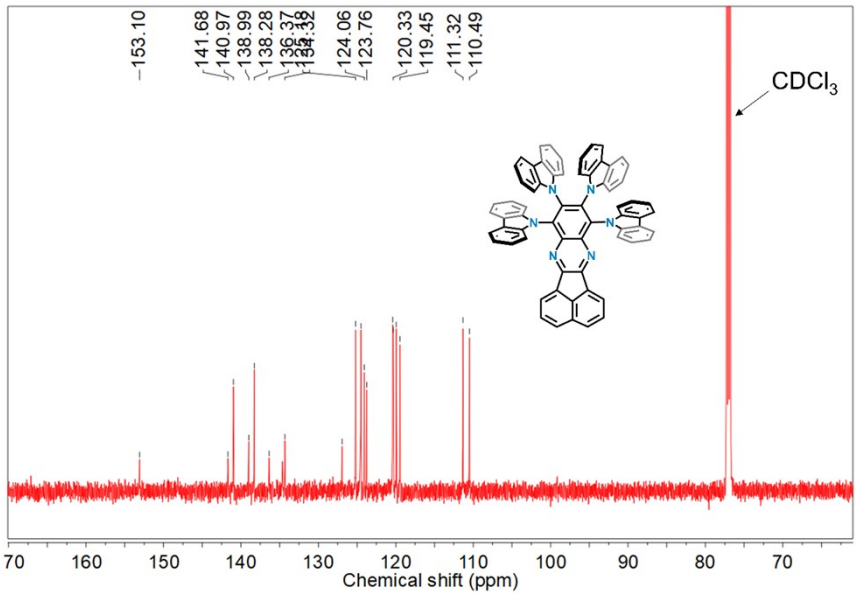

Fig. S13 ^{13}C NMR chart of **4CzAQ**.

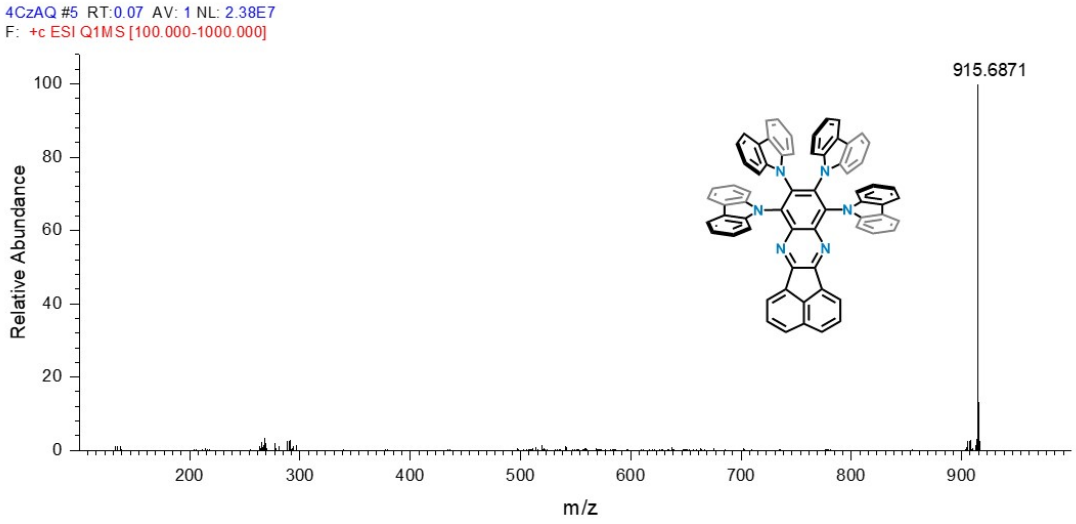

Fig. S14 MS chart of **4CzAQ**.

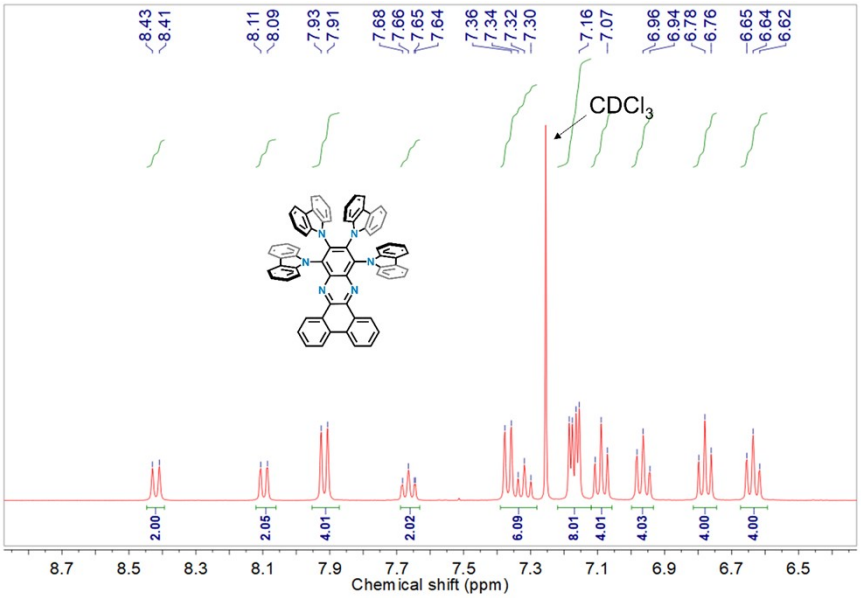

Fig. S15 ^{1}H NMR chart of **4CzDP**.

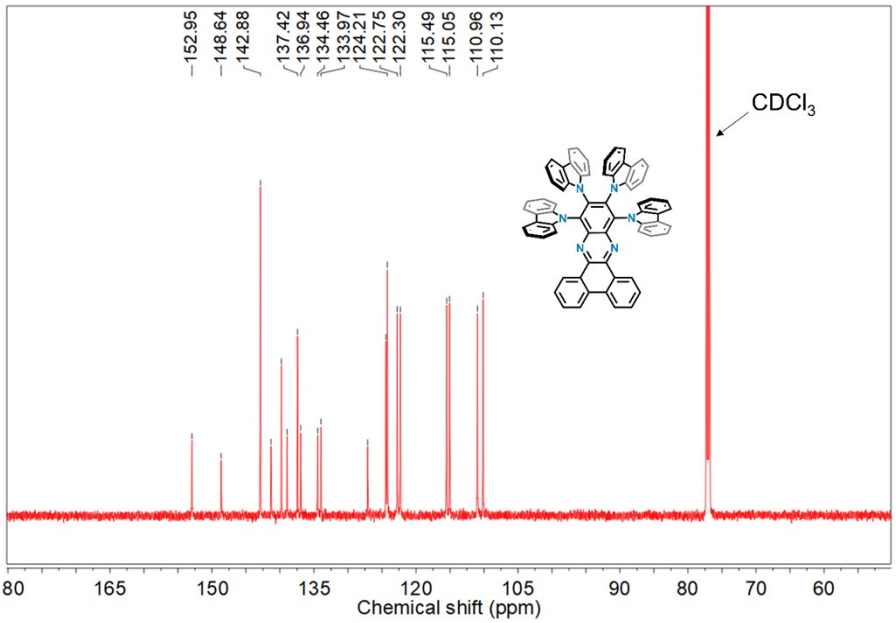

Fig. S16 ^{13}C NMR chart of **4CzDP**.

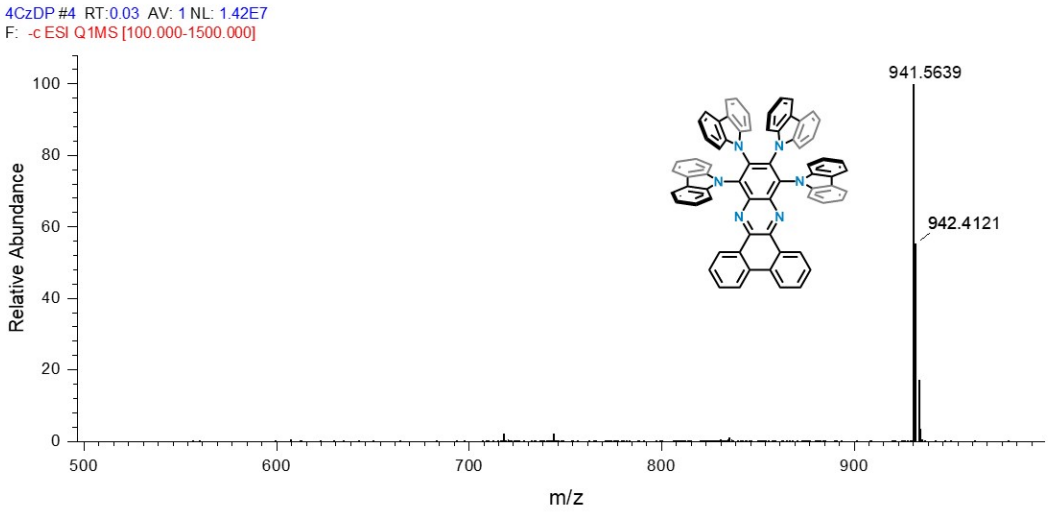

Fig. S17 MS chart of **4CzDP**.

Table S5 Crystallographic data and structure refinement for **4CzAQ**.

CCDC number	2224330
Empirical formula	$C_{68}H_{40}Cl_6N_6$
Formula weight	1153.76
Temperature	169.99(10) K
Crystal system	Monoclinic
Space group	*P*21/c
Unit cell dimensions	a=14.4428(7) Å α=90 ° b=17.4445(9) Å β=98.072(4) ° c=22.1522(11) Å γ=90 °
Volume	5525.9(5) Å^3
Z	4
ρ_{calc}	1.387 g/cm^3
F(000)	2368.0
Crystal size	0.15 × 0.11 × 0.09 mm^3
Radiation	Mo Kα (λ=0.71073)
Index ranges	-17 ≤ h ≤ 11, -15 ≤ k ≤ 20 -26 ≤ l ≤ 26
Reflections collected	24585
Independent reflections	9728 [R_{int} = 0.0287, R_{sigma} = 0.0393]
Data/restraints/parameters	9728/108/735
Goodness-of-fit on F^2	1.016
Final R indexes [I>=2σ (I)]	R_1 = 0.0739, wR_2 = 0.1890

Final R indexes [all data]	R_1 = 0.0950, wR_2 = 0.2064
Largest diff. peak/hole	0.73/-1.62 e Å^{-3}

Table S6 Crystallographic data and structure refinement for **4CzDP**.

CCDC number	2224332
Empirical formula	$C_{70}H_{44}Cl_4N_6$
Formula weight	1110.91
Temperature	149.99(10) K
Crystal system	Monoclinic
Space group	$P2_1/_C$
Unit cell dimensions	a=15.1734(4) Å α=90 ° b=17.1579(4) Å β=100.849(3) ° c=21.4227(6) Å γ=90 °
Volume	5477.6(3) Å^3
Z	4
ρ_{calc}	1.347 g/cm^3
F(000)	2296.0
Crystal size	0.14 × 0.12 × 0.1 mm^3
Radiation	Cu Kα (λ = 1.54184)
Index ranges	-18 ≤ h ≤ 18, -21 ≤ k ≤ 20, -25 ≤ l ≤ 26
Reflections collected	22116
Independent reflections	10796 [R_{int} = 0.0399, R_{sigma} = 0.0486]
Data/restraints/parameters	10796/0/721
Goodness-of-fit on F^2	1.016
Final R indexes [I>=2σ (I)]	R_1 = 0.0648, wR_2 = 0.1603
Final R indexes [all data]	R_1 = 0.0807, wR_2 = 0.1761
Largest diff. peak/hole	0.68/-0.97 e Å^{-3}

References

1 T. Lu and F. Chen, *J. Comput. Chem.*, 2012, **33**, 580–592.

2 W. Humphrey, A. Dalke and K. Schulten, *J. Mol. Graph.*, 1996, **14**, 33–38.

3 D. Zhang, M. Cai, Y. Zhang, D. Zhang and L. Duan, *Mater. Horiz.*, 2016, **3**, 145–151.

4 L.-S. Cui, A. J. Gillett, S.-F. Zhang, H. Ye, Y. Liu, X.-K. Chen, Z.-S. Lin, E. W. Evans, W. K. Myers, T. K. Ronson, H. Nakanotani, S. Reineke, J.-L. Bredas, C. Adachi and R. H. Friend, *Nat. Photonics*, 2020, **14**, 636–642.

5 F.-M. Xie, H.-Z. Li, K. Zhang, H.-Y. Wang, Y.-Q. Li and J.-X. Tang, *ACS Appl. Mater. Interfaces*, 2023, **15**, 39669–39676.

6 U. Balijapalli, M. Tanaka, M. Auffray, C.-Y. Chan, Y.-T. Lee, Y. Tsuchiya, H. Nakanotani and C. Adachi, *ACS Appl. Mater. Interfaces*, 2020, **12**, 9498–9506.
7 M. Xu, M. Liu, M. Shi, M. U. Ali, S. Jiao, W. Cao, Y.-C. Wu and H. Meng, *J. Mater. Chem. C*, 2019, **7**, 13754–13758.
8 F. Wang, X. Cao, L. Mei, X. Zhang, J. Hu and Y. Tao, *Chin. J. Chem.*, 2018, **36**, 241–246.
9 J. H. Yun, K. H. Lee, H. Jeong and J. Y. Lee, *J. Mater. Chem. C*, 2022, **10**, 10950–10956.
10 J. Jayakumar, T.-L. Wu, M.-J. Huang, P.-Y. Huang, T.-Y. Chou, H.-W. Lin and C.-H. Cheng, *ACS Appl. Mater. Interfaces*, 2019, **11**, 21042–21048.
11 J. Kim, C. W. Joo, S.-J. Woo, J. Park, J. Lee and Y.-H. Kim, *J. Mater. Chem. C*, 2022, **10**, 7304–7310.
12 G. Kreiza, D. Banevičius, J. Jovaišaitė, K. Maleckaitė, D. Gudeika, D. Volyniuk, J. V. Gražulevičius, S. Juršėnas and K. Kazlauskas, *J. Mater. Chem. C*, 2019, **7**, 11522–11531.
13 M. Mamada, H. Katagiri, C. Chan, Y. Lee, K. Goushi, H. Nakanotani, T. Hatakeyama and C. Adachi, *Adv. Funct. Mater.*, 2022, **32**, 2204352.
14 B. Madushani, M. Mamada, K. Goushi, T. B. Nguyen, H. Nakanotani, H. Kaji and C. Adachi, *Sci. Rep.*, 2023, **13**, 7644.
15 D. Hu, M. Zhu, C. Shi, W. Yuan, N. Sun, B. Huang and Y. Tao, *J. Mater. Chem. C*, 2021, **9**, 13384–13391.
16 H. Uoyama, K. Goushi, K. Shizu, H. Nomura and C. Adachi, *Nature*, 2012, **492**, 234–238.
17 X. Zhou, Y. Xiang, S. Gong, Z. Chen, F. Ni, G. Xie and C. Yang, *Chem. Commun.*, 2019, **55**, 14190–14193.